Journal of
Materials Chemistry A

Materials for energy and sustainability

Accepted Manuscript

This article can be cited before page numbers have been issued, to do this please use: P. J. J. Sagayaraj, O. Keishi , N. Okibe, A. Sengeni, H. Kim and K. Sekar, *J. Mater. Chem. A*, 2025, DOI: 10.1039/D5TA04391C.

ROYAL SOCIETY OF CHEMISTRY

rsc.li/materials-a

View Article Online
DOI: 10.1039/D5TA04391C

ARTICLE

Reconstructing the electronic structure of nickel selenide by Cu incorporation for enhanced alkaline hydrogen evolution reaction

Received 00th January 20xx,
Accepted 00th January 20xx

DOI: 10.1039/x0xx00000x

Prince JJ Sagayaraj,[a] Keishi Oyama,[b] Naoko Okibe,[b] Anantharaj Sengeni,[c*] Hyoung-il Kim,[d*] and Karthikeyan Sekar[a,d*]

Nickel selenides are proven to be the efficient electrocatalysts in catalyzing hydrogen evolution reaction (HER) for alkaline water electrolysis, but their unsatisfying durability in alkaline medium opens up for the strategic exploration in improving the HER activity over time. Tuning the electronic structure of hydrothermally synthesized nickel selenide with electrodeposited Cu (NCS/NF) has proven fruitful beyond imagination in HER for the first time. Introduction of Cu enabled this newly developed catalyst to deliver current density of -10 $mAcm^{-2}$ by requiring a lower overpotential of only 45 mV due to the enhanced electron diffusivity with an extended surface area. The voltage-induced phase transition of nickel selenide with Cu exhibited 2.5-fold increment in HER activity which enabled this activity tuned catalyst (AD NCS/NF) to surpass the state-of-the-art Pt at all potentials under identical conditions and when connected in two-cell configuration AD NCS/NF||NiFeLDH required cell voltage of only 1.48V to deliver 50 $mAcm^{-2}$. Further, XRD, XPS and XAS findings provide insights onto the voltage-induced structural reorganization of NCS/NF during the accelerated degradation test revealing the superior HER activity with the improvement of catalyst's durability over time. This unique regulation of crystalline facets in NCS/NF with Se-enriched surface promotes the intrinsic activity for striking H_2 production.

Introduction

The impending use of fossil fuels leading to imminent environmental issues and energy crisis attracts a severe demand in sustainable energy production.[1-3] Green hydrogen (H_2) through water splitting (WS) by renewable electricity is a promising alternative in powering up the world leaving just water behind.[4, 5] Although, the availability of H^+ for $2e^-$ water reduction into H_2 is abundant at pH 0, the lack of catalysts' durability, higher operational cost, and limited exploration of electroactive materials restricted the development of acidic electrolyzers on a larger scale thereby concentrating on alkaline WS at pH 14 is the need of time.[6, 7] Alkaline WS has grabbed recent attention, because, the industry oriented H_2 generation is typically alkaline and the cost involved in setting up an alkaline electrolyzer is seemingly cheaper as the catalytically active materials would be developed from earth-abundant 3d-transition metals.[8-10] Despite the intrinsic improvement of sluggish kinetics associated with $4e^-$ OER by forming oxyhydroxide bonds (*O-OH) with 3d-transition metals (TM), the water dissociation coupled, proton abstraction step in alkaline HER impedes the overall efficacy of the WS in alkaline medium.[11-13] Even, the benchmark Pt, struggles to dissociate H_2O.[14, 15] 3d-TM are significant for their efficiency in dissociating water in alkaline medium but fails to catalyze HER and affects the overall kinetics.[16-19] In this regard, modulating the electronic structure of 3d-TM could help in achieving lower overpotential and higher current density.

TM selenides are a class of chalcogenides having selenium (Se) atom whose electronegativity (2.55) shows greater tendency to covalently bond with metals inducing *in situ* defects with non-stoichiometric compound formation for better charge carrier characteristics.[20-25] Among those, nickel selenides are the most explored electrocatalysts for HER because of their intrinsic metallic anion properties that come with selenium (Se).[21, 26-28] Also, Ni as an atom shows better philicity towards hydride ion.[29, 30] On increasing the number of Se atoms, the accessibility of H^+ on electrochemically active Se sites gets enhanced and the Ni atom as an H^- provides an easier pathway for HER in alkaline medium but suffer from poor kinetics and stability.[31, 32] To improve the stability and charge transfer kinetics, constructing an interface with another metal imparting more metallic character to nickel selenides is inevitable.[33, 34] Several reports of bi/multi-metallic selenides[35, 36] have been utilized in the recent past for splitting water, synergistically supplementing the structure deficit inert sites towards HER comparing their individual counterparts.[27, 37-39] Cu is an earth abundant 3d TM whose addition to other electroactive materials have shown to improve their catalytic activity and

[a] Department of Chemistry, SRM Institute of Science and Technology, Chennai 603203, India
[b] Department of Earth Resources Engineering, Kyushu University, Fukuoka 819-0395, Japan.
[c] Department of Chemistry, Indian Institute of Technology, Kanpur, Uttar Pradesh 208016, India
[d] Department of Civil & Environmental Engineering, Yonsei University, Seoul 03722, Republic of Korea
E-mail: karthiks@yonsei.ac.kr
† Footnotes relating to the title and/or authors should appear here.
Supplementary Information available: [details of any supplementary information available should be included here]. See DOI: 10.1039/x0xx00000x

View Article Online
DOI: 10.1039/D5TA04370C

kinetics. [40-42] Due to Cu's extreme instability and susceptibility to oxidation on its surface, the subsurface concentration of Cu primarily shows the promising critical activity of HER.[43] On alloying, or interfacing Cu with other material, the subsurface concentration of Cu in the bulk influence the surface electronic properties as the diffusion of electrons from bulk to surface is promoted leading to improved activity.[44] Moreover, Cu modified TM selenide heterostructures boosted the HER activity wherein the interface engineering between the d-electron sufficient Cu atom and M_xSe_y (M-3d TM) synergistically induce improvements in their electronic structure optimal for reactant interaction in alkaline medium for dissociating H_2O.[45-47] Despite these advancements in designing HER active catalysts, identifying the origin of real active species and understanding the structural transformation of the electrocatalyst under HER operating conditions is highly essential for ensuring the durability of the electroactive materials and is often neglected in research hotspot.[48-50] Researchers have been intriguingly reporting the dynamic phase evolution and self-re-orientation of the catalyst to understand the HER mechanism and origin of cathodic materials.[30, 51, 52]

Motivated with these insights, we first synthesized nickel selenide in selenium rich phase $NiSe_2$ utilizing a simple hydrothermal technique, as the traditional methods including solid-state synthesis, elemental direct reaction, alloying involves the usage of toxic-metal metal precursors, reducing agents and the subjection of higher temperatures, which would affect its ease of scalability. Then, the electronic structure and the atomic framework of the hydrothermally constructed nickel selenide on Ni foam is modified with Copper (Cu) layer (NCS/NF), where the Cu is deposited by dynamic hydrogen bubble template (DHBT) method. The electrodeposited Cu on Ni foam offered the substrate to be more porous with hierarchically modified 3D structure promoting the diffusion kinetics. The fascinating electrochemical HER activity between porous Cu foam and nickel selenide electronically communicating through Se atoms profounds to be extremely

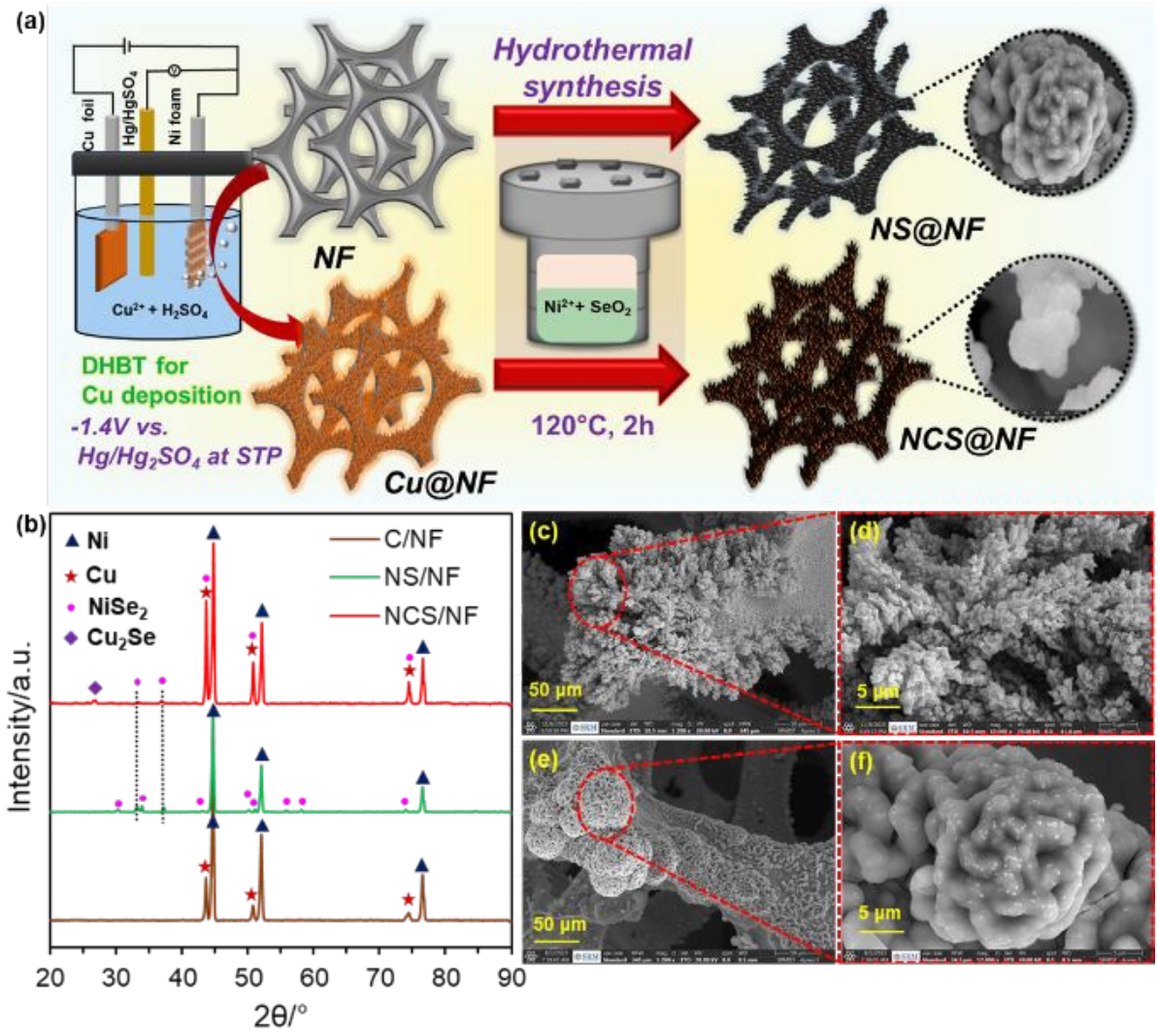

Fig.1 (a) Schematic illustration for the synthesis of different self-supporting electrocatalysts, (b) XRD pattern for C/NF, NS/NF and NCS catalyst, FE-SEM images of (c-d) C/NF and (e-f) NS/NF respectively under higher magnification.

responsive to alkaline HER requiring only 45mV of overpotential to deliver the cathodic current density of -10 $mAcm^{-2}$. Achieving 2.5-fold improvement in HER activity over time at pH 14, NCS/NF catalyst outperforms Pt on all reduction potential under similar reductive conditions and in two-electrode system too. Post HER studies subsequently infer on the electronic structure reconstruction during the cathodic reduction process.
combination fitting analysis.

Results and discussion

The outline for the synthesis is given in Fig. 1a. Under hydrothermal conditions at 120°C, the Ni foam liberates Ni^{2+} ions slowly, whose lost electrons reduces the hydrolysed SeO_2 to form selenide anions which then nucleates with Ni^{2+} in the solution forming nickel selenide. Initially, the hydrolysed SeO_2 forms selenous acid which on further reduction forms selenide anion.[53] As the reaction proceeds, the autoclave develops pressure within it by time. Also, the pH of the reaction mixture reduces to near acidic which favours the dimerization of selenide anions forming diselenides. In the presence of Cu deposited NF (C/NF), Cu^+ being a soft acid is prone to interact with soft bases like S and Se having more likeliness to form Cu_2Se which is eventually bonded chemically with $NiSe_2$. The selenised catalysts and their crystalline phases were determined by Powder Xray Diffraction (PXRD) (Fig. 1b). All of them showed the presence of bare Ni foam peaks at 44.6°, 51.9°, and 76.5° for the *hkl* planes (111), (200) and (220) respectively (JCPDS card no 01-070-0989), and the electrode that was deposited with DHBT Cu exhibited additional Cu peaks at 2θ= 43.4° (hkl;111), 50.6°(hkl;200), and 74.6° (hkl;220) (JCPDS card no 01-1242) with no alloying features with the Ni foam. The crystal planes diffracted from NS/NF were matching well with the cubic phase of $NiSe_2$ (JCPDS no. 11-0552 and 08-0423; Space group- Pa3; Space number -205) indicating the formation of nickel selenide. The Cu deposited NF (NCS/NF) shows an additional Cu_2Se peak at 2θ = 26.7° with (111) plane (JCPDS no. 03-065-2982) along with cubic $NiSe_2$ peaks, as Cu atoms on the surface has higher tendency to interact with the Se atoms under the hydrothermal conditions.[54] The method that has been presented enables the effective synthesis of nickel selenide without the use of high temperatures or any other reducing agents, as can be shown in Table S1 for comparison.

Field Emission Scanning Electron Microscopy (FE-SEM) is performed to determine the morphology of the electrocatalysts. The highly porous dendritic structures obtained for C/NF (Fig. 1c and d) compared to bare NF (Fig. S1) vouched for improved hydrophilicity and the increased surface roughness that were crucial for improved electrochemical surface area (ECSA). The morphology variation of nickel selenides in the presence (Fig. 2a and b) of porous Cu is clearly visible, that the NCS/NF is obtained with three dimensional thin-wrinkled sheets on porous Cu surface exposing more active sites, whereas FESEM images of NS/NF (Fig. 1e and f) seemed to be dwindled with limited exposure of active sites. Transmission electron microscopy (TEM) (Fig. 2c) with the inset verifies thin sheet like open structures (as seen from SEM) with the exposure of crystalline planes (210) of $NiSe_2$ and (111) Cu_2Se in NCS/NF

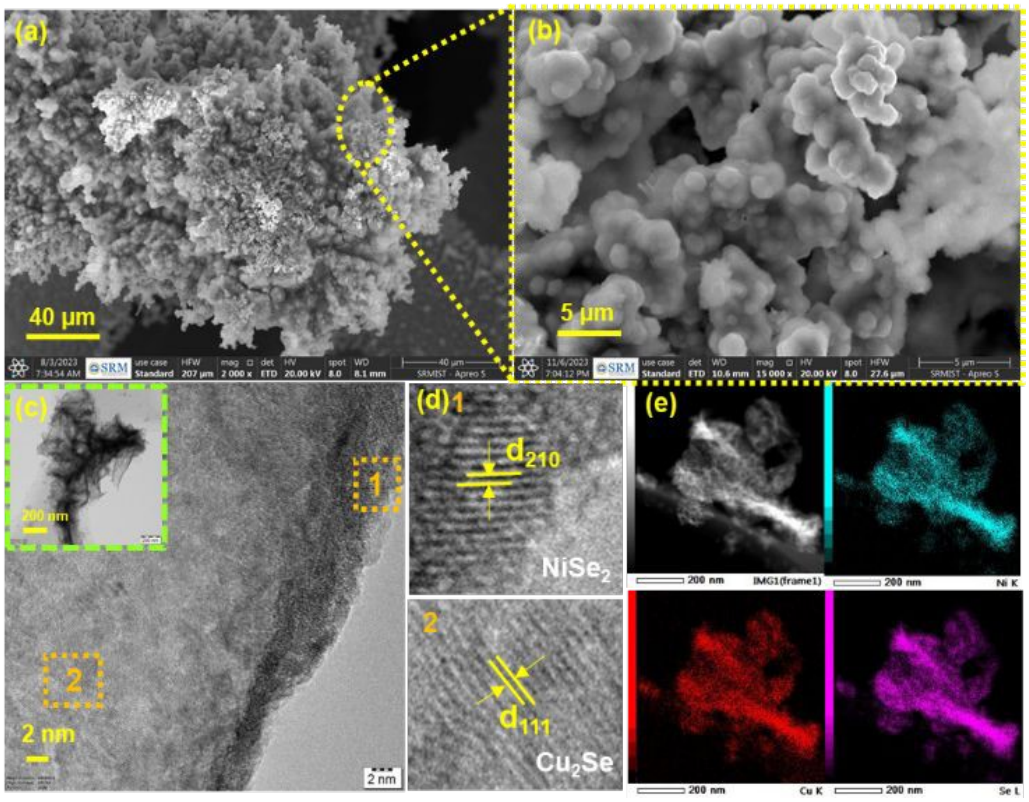

Fig. 2. (a and b) FE-SEM, (c) TEM, (d) HR-TEM and (e) STEM Elemental mapping of Ni, Cu and Se respectively for the catalyst NCS/NF.

View Article Online
DOI: 10.1039/D5TA04391C

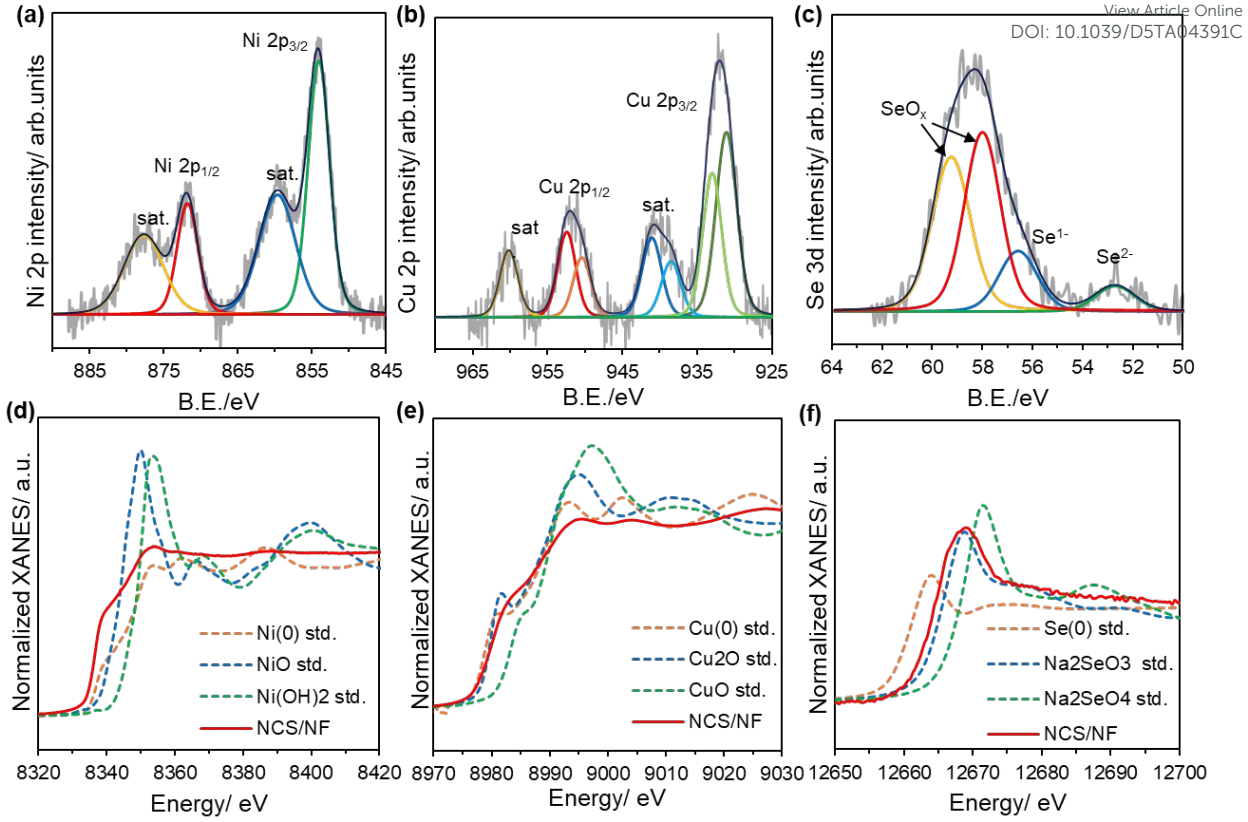

Fig. 3. Core level spectra of (a) Ni 2p, (b) Cu 2p, (c) Se 3d, XANES spectra of (d) Ni K edge, (e) Cu K edge and (f) Se K edge for NCS/NF catalyst respectively.

catalyst. High-resolution (HR-TEM) and Dark-field Scanning (STEM)- Energy dispersive Xray (EDX) elemental mapping (Fig. 2d and e) confirmed the formation of crystalline planes with d-spacing matching with that of $NiSe_2$ and Cu_2Se as confirmed from XRD and the atomic distribution of Cu, Ni and Se atoms is homogeneous all over the catalyst surface. STEM image and the corresponding Selected Area Electron Diffraction (SAED) pattern (Fig. S2) with sharp rings showed high poly-crystalline nature of NCS/NF confirming the existence of cubic selenides. The surface of the bare NF is modified from its pristinely hydrophobic (Fig. S3) to super hydrophilic after the selenisation in both NS/NF and NCS/NF catalysts (Fig. S4 and S5). The smaller contact angle of 0° between the water droplet and electrocatalysts exhibit reduced bubble adherence which also improves better facilitation of mass transfer and reduction in intrinsic resistance. (Video S1-S2).

To further explore on the structural characteristics of NCS/NF, Xray Photoelectron Spectra (XPS) was done with the survey scan (Fig. S6) showing the presence of Ni, Cu, Se and O atoms. The increased concentration of O on the surface is due surface oxidation. In Fig. 3a, core-level Ni 2p spectrum has a strong Ni $2p_{3/2}$ and Ni $2p_{1/2}$ peaks at binding energies (BE) 855.3 (±0.2 eV) and 872.6 (±0.2 eV) respectively, attributing to the presence of Ni^{2+} from $NiSe_2$ along with the presence of shake-up satellites. The mixed valence states of porous Cu is depicted in Fig. 3b. Cu 2p exhibits Cu $2p_{3/2}$ and Cu $2p_{1/2}$ with the additional satellites corresponding to the presence of oxidised copper in NCS/NF. Further, Cu $2p_{3/2}$ is deconvoluted into two peaks at 931.7 (±0.2 eV) and 933.8 (±0.2 eV) due to the existence of +1, +2 oxidation states coordinating with Se and adsorbed O atoms on the surface. The presence of selenide anions is implied in the Se 3d core-level spectrum (Fig. 3c) which showcased the presence of Se in the most anionic form and is extremely negative shifted due to higher electron density states around Se atoms from Ni^{2+} and Cu^{2+}/Cu^{+} respectively. The BE at 56.7 (±0.2 eV) could be originated from selenide anion of $NiSe_2$ and Cu_2Se and the peaks with positive shifted BE values at 58.2 (±0.2 eV), 59.3 (±0.2 eV) denotes the impurities of selenium dioxide that has been hydrolysed and reducing to from respective metal selenides. Further examination on the bulk structures and electronic states of NCS/NF was done by Xray Absorption Spectral (XAS) analyses. The Ni K edge Xray Absorption Near Edge Spectra (XANES) displayed in Fig. 3d shows distinct spectra from Ni (0) and Ni (+2) with decreased amplitude featuring the presence of Ni^{2+} of $NiSe_2$ and the disordered crystal structure. Then, the Fourier transformed Extended X-ray Absorption Fine Structure (FT-EXAFS) of NCS/NF (Fig. S7a) Ni-K edge clearly has a coordination peak at 2.42Å fitted in R space, revealing the presence of shortened Ni-Se bonds as the electron dense Se atom tends to be more anionic and forms stronger bond with Ni^{2+} which is in great agreement with the XRD, HRTEM and XPS results. Correlatively, the local chemical environment of Cu is confirmed from the pre-edge of Cu K edge XANES (Fig. 3e) signifying that the oxidized Cu that has been formed during selenization process, existed in mixed oxidation states with the FT-EXAFS (Fig. S7b) fitted in Cu R space revealing the presence

View Article Online
DOI: 10.1039/D5TA04391C

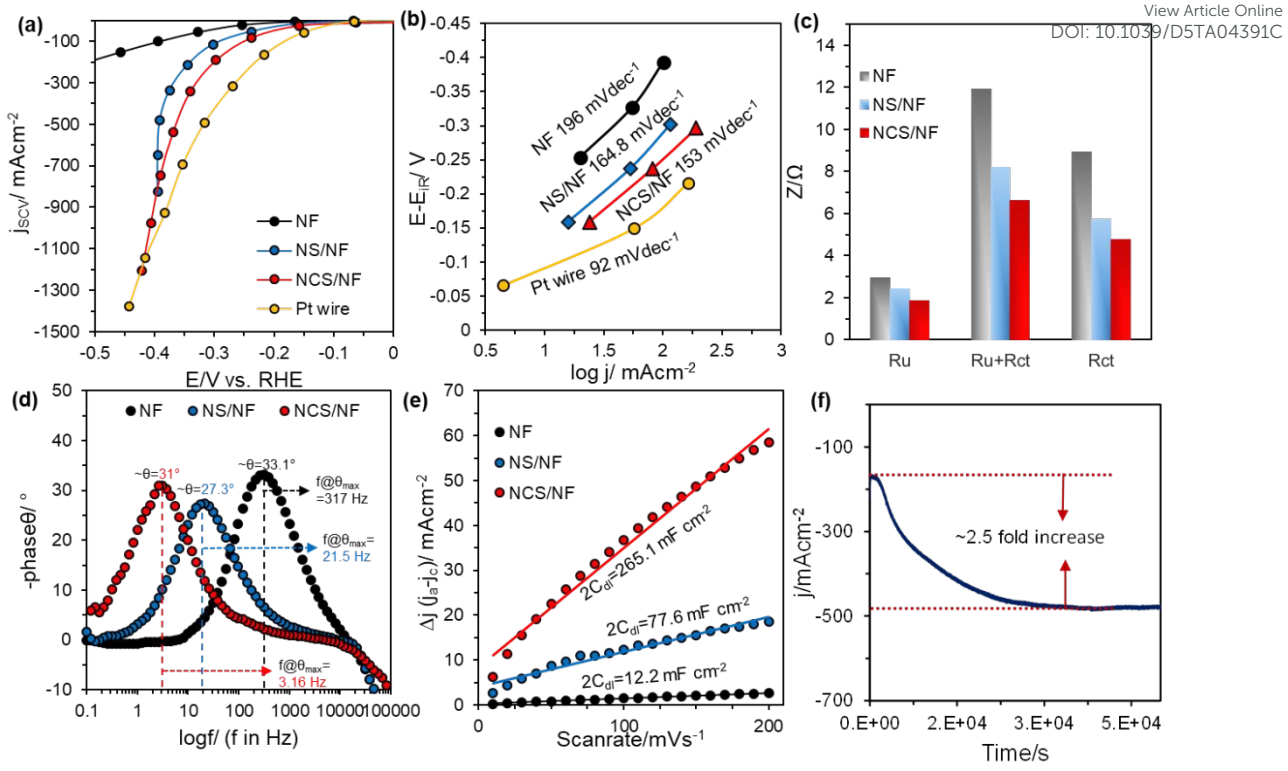

Fig. 4. (a) Polarisation curves (SCV) for HER studies with maximum iR drop compensation, (b) Tafel plot, (c) Comparative chart depicting the uncompensated and charge-transfer resistances, (d) Bode-phase angle plot showing phase shift and their corresponding frequency values for various electrocatalysts, (e) Linear C_{dl} plot of non- Faradaic charging current density vs. scan rate for NF, NS/NF and NCS/NF respectively and (f) Accelerated degradation plot for NCS/NF catalyst

of Cu-O and Cu-Se bonds with extended bond lengths, 2.62Å and 1.9Å respectively. This evidently supports the transfer of electrons from Cu to Se then to Ni-Se occurring during reduction reaction towards metal selenide formation under hydrothermal conditions. The Se K edge XANES (Fig. 3f) gets shifted to higher energies due to the increase in valence states accounting for the formation of bonds with Ni and Cu. All the XANES spectra have lowered intensity than their corresponding references ensuring the creation of disorders within the crystal system due to the co-existence of Ni, Cu and Se atoms.[55]

Utilizing a conventional technique of three-electrode configuration, the electrochemical activity for 2e$^-$ reduction of H_2O is tested for the catalytic materials NS/NF, NCS/NF in comparison with bare NF and Pt wire at basic pH of 14. The Linear Sweep Voltammogram (LSV) (Fig. S8) studies exhibited higher HER activity for NCS/NF with improved kinetics. The incorporation of Cu interplayed the role of H_2O adsorption and charge transfer kinetics activating the kinetics of NCS/NF than NS/NF and bare NF. To investigate the real HER activity Sample Current Voltammogram (SCV)[56] is demonstrated for all the materials by deriving from their individual *i-t* curves (Fig. S9a-d), at a region where the double layer charging diminishes. Fig. 4a SCV plot shows that, NCS/NF material showed superior activity reaching a current density of -1.2 A cm^{-2} at maximum vertex potential which is 31% greater than NS/NF. Also, the overpotential required for delivering -10 mA cm^{-2} (η_{10}) is just 45mV for NCS/NF and 124 mV for NS/NF which are better than bare NF (η_{10} = 208mV). As seen from the comparison chart (Fig. S10), both NS/NF and NCS/NF are seemingly active towards HER, because the atoms arranged in cubic $NiSe_2$ have greater packing fraction with more chances of hydrogen adsorption on the neighbouring active sites leading to the evolution of H_2.[57]

The interplay of porous Cu in its selenized form improved the mass transfer of the catalytic system, as noted for its high electron transport efficiency and hydrophilicity. The value of Tafel slope (Fig. 4b) also reflects on the same as NCS/NF (153 mV dec^{-1}) has lower Tafel value than NS/NF (164.8 mV dec^{-1}) and Pt (92 mV dec^{-1}) exhibiting rapid water dissociation kinetics which is the rate limiting step in alkaline HER. With significant activation of HER sites promoting the dissociation of water and concurrent H_{ads} discharge electrochemically, the charge-transfer resistance along the electrode (catalytic material)-electrolyte interface is perceived to be essential and was studied using Electrochemical Impedance Spectroscopy (EIS) under catalytic turnover conditions. Nyquist and Bode-impedance plots (Fig. S11) suggest that NCS/NF perform better than NS/NF with lowering charge transfer resistance (R_{ct}) of 4.76Ω and for NS/NF the R_{ct} value is 5.75Ω following the same trend for uncompensated resistance (R_u) (R_u; NCS/NF-1.86Ω & NS/NF-2.43Ω) (Fig. 4c). The reduction of R_u supports that inclusion of porous Cu facilitates the detachment of HER gas bubbles and wettability of electrode materials. The Bode-phase angle plot (Fig. 4d), conclusively exhibits all the phase shift values <45° supporting the 2e$^-$ transfer kinetic behaviour for HER. The frequency at which phase shift occurs gets lowered for NCS/NF (3.16 Hz) than NS/NF (21.5 Hz) which is a direct

View Article Online
DOI: 10.1039/D5TA04391C

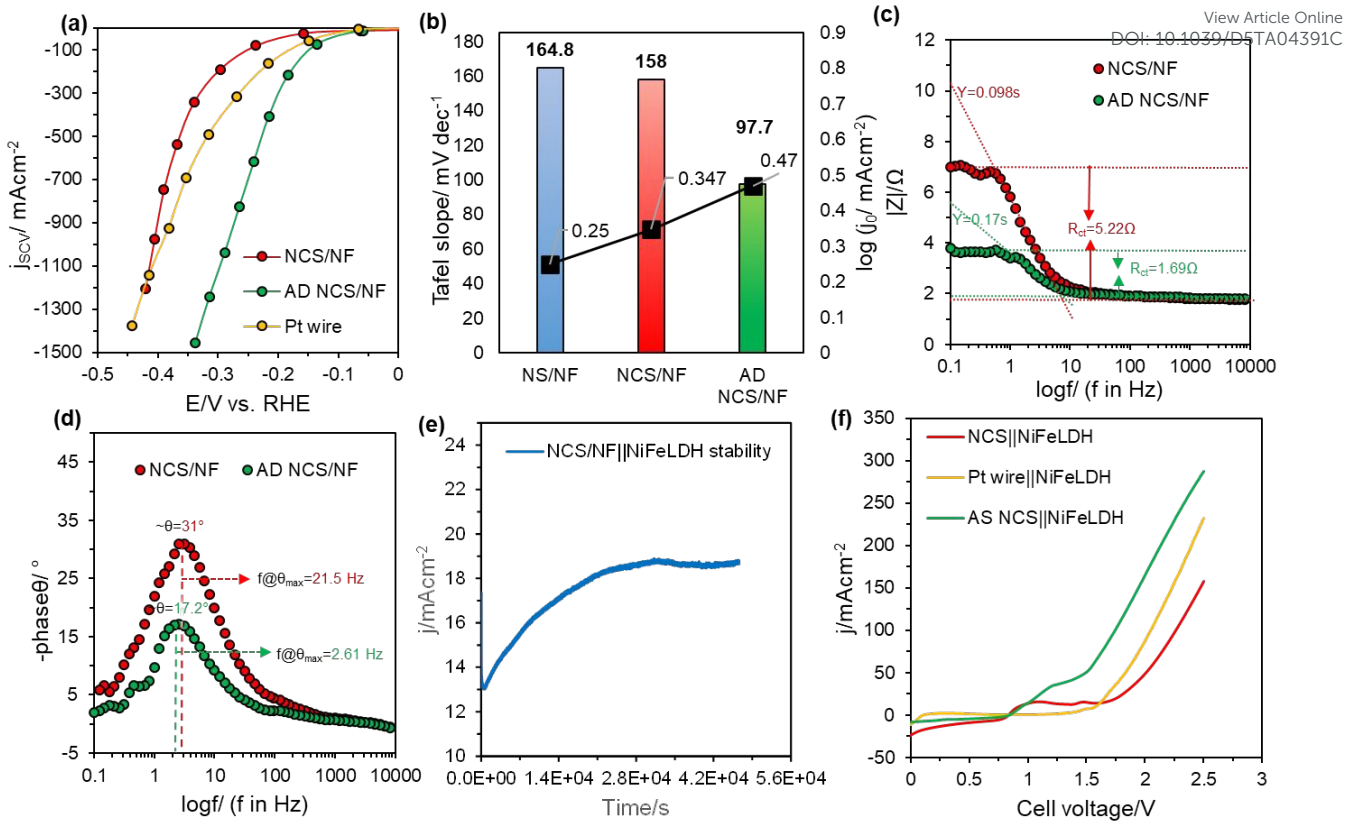

Fig. 5. (a) SCV plot after HER studies with 100% iR compensation, (b) Comparison plot for Tafel slope values and exchange current density, (c) Bode-absolute impedance plot and (d) Bode-phase angle plot showing phase shift and their corresponding frequency values for NCS/NF and AD NCS/NF catalysts, (e) Two-electrode stability curves of NCS/NF as the cathode (-) and NiFeLDH as the anode (+) in 1.0M KOH and (f) Polarisation curves in two-electrode system

indicative for the improved ECSA on incorporating porous Cu. The double layer capacitance is also calculated for all the materials using C_{dl} method. The linear plot of scan rate vs. current density constructed from CVs recorded in non-faradaic region (Fig. S12a-c) is given in the Fig. 4e. The extreme improvement in the $2C_{dl}$ values (12.2, 77.6 and 265.1 mFcm^{-2} for bare NF, NS/NF and NCS/NF respectively) underpins the enhancement in ECSA. With porous Cu, $NiSe_2$ was able to carry-out alkaline HER having all the results in good agreement with the polarisation and Tafel values in comparison with Pt. To check the durability of the highly active NCS/NF and to withstand the long-term HER operating conditions, accelerated degradation (AD) test is performed in 1.0M KOH at a fixed potential of -1.3V against Hg/HgO reference electrode and Ni foam as counter electrode (Fig. 4f). Initially, NCS/NF delivered a current density of -172 mAcm^{-2}, with gradual increase in the activity by 2.5-fold within 28400 s and further showed negligible degradation. The increment in the current density is indeed an indication for the deep activation with the evolution of real active sites involving structural reconstruction during prolonged HER electrolysis, after which it is observed that the current density keeps relatively stable without noticeable degradation demonstrating the long-term stability of the catalyst.

To delve more, NCS/NF after AD (AD NCS/NF) is examined for electrochemical reproducibility. It is evident from the SCV plot (Fig. 5a) derived from the *i-t* curves of Fig. S13a, that the material was visibly outperforming Pt at all reductive potentials with requiring only -0.337V vs. RHE to reach the maximum current density of 1.45 Acm^{-2} while Pt required -0.45V vs. RHE for the same. On comparing the HER activity alongside the kinetics of AD NCS/NF, the extracted Tafel slope is found to be lowered (97.7 mV dec^{-1}) following Volmer-Heyrovksy mechanism[58] (Fig. S13b) which is entirely different from the rate limiting step followed by NS/NF (water-dissociation step). This suggests that AD NCS/NF went through surface reconstruction with the evolution of new active sites that is entirely different from that of $NiSe_2$ and NCS/NF and is intrinsically activating with greater exchange current density values (j_0) (Fig. 5b). Depicting the same trend, the charge transfer kinetics of AD NCS/NF material evidenced from the EIS results, profounds the lowered R_{ct} value of 1.69Ω as measured from Nyquist plot (Fig. S13c). The Bode-absolute impedance plot (Fig. 5c) also signifies the reduction in R_{ct} value and further, the admittance at the lowest frequency of operation was also higher for AD NCS/NF (0.17s) than NCS/NF (0.098s) ascertaining better charge transfer character imparted by the intrinsic activation of the catalyst. From the Bode phase angle plot (Fig. 5d), phase shift values are lesser than 45°, eventually confirming the kinetically controlled HER reaction and the lowest θ=17.2° (2.61 Hz) observed for AD NCS/NF hints the retainment of ECSA when compared to that of NCS/NF, θ=31° (21.5 Hz). In contrast the $2C_{dl}$ value is increased to 447.4 mF cm^{-2} (Fig. S14). From these results, it is obvious that the enhanced HER activity during AD test, made significant transformation in the crystal structure thus intrinsically

View Article Online DOI: 10.1039/D5TA04791C

activating NCS/NF in retaining the ECSA. Based on the above results, the NCS/NF catalysts after stability exhibited better HER activity and the catalyst is tested for overall water splitting in 1.0M KOH at room temperature utilizing NCS/NF as the cathode and a NiFe layered double hydroxide (LDH) coated on Ni foam as the anodic electrode. The NCS/NF||NiFeLDH electrolyser exhibited stability with improvement in the current density as shown in Fig. 5e which is due to the voltage-induced activation of NCS/NF catalyst as observed in the half-cell analysis using three-electrode cell configuration. This confirms that NCS/NF catalyst exhibits voltage induced activation when subjected for overall electrolytic performance. Further, Fig. 5f demonstrates that the overall cell voltage required by AS NCS/NF||NiFeLDH catalyst to deliver the current density of 50 $mAcm^{-2}$ is 1.48V, wherein before stability the cell voltage is 2V and the Pt/C||NiFeLDH catalyst required 1.83V. The AS NCS/NF||NiFeLDH outperforms the benchmark Pt wire||NiFeLDH in terms of overall water splitting as observed from the half-cell HER studies. The remarkable activity of the NCS/NF catalyst in two-electrode systems is due to the nickel selenide framework and its interaction with the Cu, which optimizes the adsorption strength of intermediates for HER showing that the NCS/NF electrode has great promise for use in real-world alkaline water electrolysis.

To explore into structural and morphology changes, FESEM is taken after HER (Fig. 6b and c). There is a slight variation in the morphology of NCS/NF with more agglomerated structures. The STEM elemental mapping in dark mode also supports the morphology variation and showed the presence of Ni, Cu and Se atoms that is uniformly distributed all over AD NCS/NF (Fig. 6d). The XRD pattern (Fig. 6a) after HER has diffraction peaks at 2θ=32.7°, 44.2°, 49.7°, 59.3° and 60.8° corresponding to (101), (102), (110), (103) and (201) planes respectively associated to the hexagonal phase NiSe matching with the JCPDS pattern 03-065-3425. The additional peak at 2θ=35.9° is diffracted due to the cubic crystallisation of copper selenide matching with the reference pattern having JCPDS card no: 026-1115. It is substantiated that nickel diselenide under HER conditions, undergoes phase evolution as the Se_2^{2-} dimer bond breaks forming bond with nearby Ni^{2+} atoms and the leached-out Se atom from the cubic phase of $NiSe_2$ interacts with the Cu.[59, 60] The Cu_2Se under cathodic reduction potential is expected to form metallic Cu aggregates which on further interaction with the Se nucleates forming $CuSe_2$. Both NiSe and $CuSe_2$ is a HER active catalyst, whereas in NiSe the d-band centre shifts-up closer to Pt-like.[61] Unlike conventional catalysts, the HER bubbles evolved from the surface of the catalyst during the process of electrolysis didn't affect the overall electrochemical activity, rather achieved higher levels of activity. This is attributed to the improved surface properties thereby reducing the resistance that exists between the electrolyte and the electrode interface as corroborated from the contact angle measurements of AD NCS/NF (Fig. S15). It is observed that super hydrophilic behaviour was retained when a water drop was suspended on its surface and absorbed quickly without any contact angle (0°) (Video. S3).

Fig. 7a illustrates the schematic representation for the phase transformation of NCS/NF under prolonged electrolysis. The core-level XPS for AD NCS/NF is demonstrated where the Ni 2p spectra (Fig. S16a) has Ni $2p_{3/2}$ peak at BE 856.1 (±0.2 eV) and Ni $2p_{1/2}$ at 873.3 (±0.2 eV) showing a slight positive shift, because it is very difficult to remove an electron from Ni in NiSe as, Ni^{2+} becomes more electropositive when bonded with more electronegative Se^{2-}. The Cu 2p spectra (Fig. S16b) looks similar before AD test but the intensity of satellite peaks gets reduced as Cu after the exposure of reduction conditions. The Cu $2p_{3/2}$ with the three deconvoluted peaks 931.5 (±0.2 eV), 933.0 (±0.2 eV) and 935.3 (±0.2 eV) confirms the mixed valence Cu atoms with 0, +1 and +2 states respectively. The more positive shift in +2 state accounts for the formation of Cu-Se bonds. The

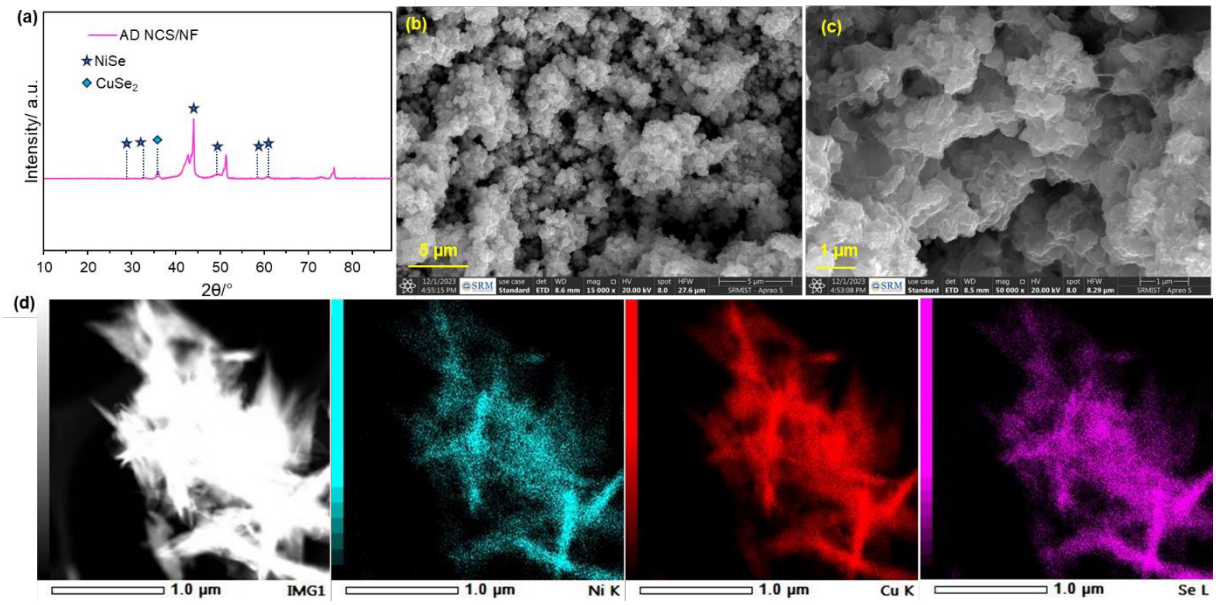

Fig. 6. (a) XRD pattern of AD NCS/NF after stability, (b,c) FESEM images and (d) STEM elemental mapping for the elements Ni, Cu and Se of NCS/NF after HER.

View Article Online
DOI: 10.1039/D5TA04501G

formation of new Cu-Se bonds is responsible for the replenishment of new active sites promoting the charge transfer abilities as per EIS results. The Se 3d core-level spectra is exhibited in Fig. S16c. The peaks at 54.5 (±0.2 eV) and 57.2 (±0.2 eV) shows the presence of diselenides and monoselenide on the surface of the catalyst, respectively alongside the oxidized Se atoms. The positive shift of Se^{-1} is due to the fact that the charge is not accumulated on Se atom and gets transferred throughout the system between Ni and Cu atoms. The peak intensity is also higher for AD NCS/NF due to the evolution of more Se atoms on the surface. To further know more about bulk properties, XAS studies have been performed after AD tests for NCS/NF. The XANES spectra for Ni K edge (Fig. S17a) resulted in the existence of Ni in +2 state. The pre-edge of Cu K edge XANES spectra enunciates that Cu exists in its reduced state with its intensity maxima matching to that of 2+ thus, proving the existence of Cu is mixed valence states (Fig. S17b). The FT EXAFS of Ni K edge fitted in R space showed the presence of Ni-Se bonds in AD NCS/NF with the radii value 2.43Å (Fig. 7b and c). This is in consistent with the hexagonal NiSe value and the bond becomes shortened due to the disorderness created within the system.[45, 62] All these results supported the phase transformation of nickel selenide during the prolonged HER conditions and this evolution of real active sites with electron-d band structure similar to Pt exhibits supreme HER activity.

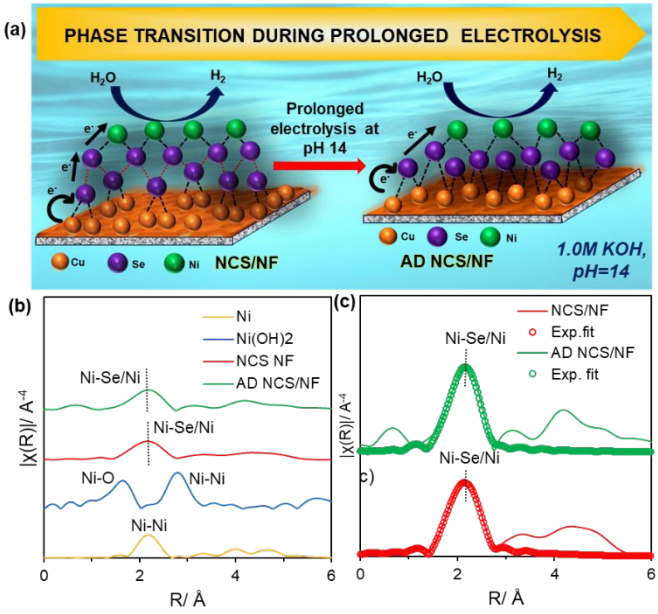

Fig. 7. (a) Scheme illustrating phase transformation of NCS/NF during prolonged HER conditions (b) EXAFS spectra for Ni K edge and (c) the corresponding FT-EXAFS fitting spectra for NCS/NF and AD NCS/NF respectively.

Conclusions

A nickel selenide system whose electronic structure is modified via hydrothermal treatment with the pre-deposited Cu layer is investigated for HER studies in alkaline medium. Hydrothermal treatment markedly accelerated the selenisation process regulating the formation of defined crystal facets. This newly developed NCS/NF catalyst required only 45mV to deliver current density of -10 $mAcm^{-2}$ due the increased SA from the coexistence of copper selenides and nickel selenides on the surface. Accelerated degradation test revealed the superior HER activity with the improvement the catalysts' durability of 2.5fold with time from phase transferred cubic $NiSe_2$ to hexagonal NiSe. The voltage-induced activation is demonstrated in two-electrode overall water electrolysis, where the AD NCS/NF||NiFeLDH required cell voltage of 1.48V for 50$mAcm^{-2}$ surpassing Pt wire||NiFeLDH. XRD, XPS and XAS findings provide insights onto the structural reorganization of NCS/NF with the ongoing HER which infers that the unique regulation of crystalline facets in NCS/NF with Se-enriched Ni and Cu surface promotes the intrinsic activity for striking H_2 production.

Author contributions

P.J.J.S. Conceptualisation, Data Curation, Methodology, Validation, Visualization, Formal analysis, Investigation, Writing – Original Draft, and writing – review & editing. K.O & N.O Funding Acquisition, Methodology, Review & Editing. A.S Formal analysis, Methodology, Validation, Visualization, Review & Editing – Original Draft. H.Kim, Review & Editing. S.K. Formal analysis, Funding Acquisition, Methodology, Validation, Visualization, Supervision, Review & Editing – Original Draft.

Conflicts of interest

There are no conflicts to declare.

Data availability

All supporting data of this article including experimental details are given in the Supplementary Information (S.I). Video S1, S2 and S3 denoting the Contact angle measurements for NS/NF, NCS/NF and AD NCS/NF catalysts respectively is provided alongside S.I.

Acknowledgements

K. S. would like to thank the Royal Society-Newton International Fellowship Alumni follow-on funding support AL\211016 and AL\221024, SERB Start-up Research Grant (SRG/2023/000658), National Research Foundation of Korea (RS-2024-00441750) and Department of Chemistry at SRMIST. P.JJ. S would like to thank Mr. Kavinkumar and Mr. Aravind (SRMIST) for their valuable support in performing catalytic studies. We acknowledge Nanotechnology Research Centre (NRC), SRMIST and SRM SCIF for providing the research facilities.

References

1. L. Nascimento, C. Godinho, T. Kuramochi, M. Moisio, M. den Elzen and N. Höhne, *Nature Reviews Earth & Environment*, 2024, **5**, 255-257.
2. P. J. J. Sagayaraj, A. Augustin, M. Shanmugam, B. Honnappa, T. S. Natarajan, K. Wilson, A. F. Lee and K. Sekar, *Energy Technology*, 2023, **11**, 2300563.
3. M. S. Faber and S. Jin, *Energy & Environmental Science*, 2014, **7**, 3519-3542.
4. Z. W. Seh, J. Kibsgaard, C. F. Dickens, I. Chorkendorff, J. K. Nørskov and T. F. Jaramillo, *Science*, 2017, **355**, eaad4998.
5. X. Zhang, C. Cao, T. Ling, C. Ye, J. Lu and J. Shan, *Advanced Energy Materials*, 2024, **14**, 2402633.
6. Y. Du, J. Liu, J. Chen, S. Wang, Y. Tang, A.-L. Wang, G. Fu and X. F. Lu, *Advanced Energy Materials*, **n/a**, 2404113.
7. J. Durst, A. Siebel, C. Simon, F. Hasché, J. Herranz and H. A. Gasteiger, *Energy & Environmental Science*, 2014, **7**, 2255-2260.
8. P. J. J. Sagayaraj and K. Sekar, *Chemical Communications*, 2024, **60**, 6817-6820.
9. L.-N. Zhang, R. Li, H.-Y. Zang, H.-Q. Tan, Z.-H. Kang, Y.-H. Wang and Y.-G. Li, *Energy & Environmental Science*, 2021, **14**, 6191-6210.
10. M. Chatenet, B. G. Pollet, D. R. Dekel, F. Dionigi, J. Deseure, P. Millet, R. D. Braatz, M. Z. Bazant, M. Eikerling, I. Staffell, P. Balcombe, Y. Shao-Horn and H. Schäfer, *Chemical Society Reviews*, 2022, **51**, 4583-4762.
11. X. Ding, D. Liu, P. Zhao, X. Chen, H. Wang, F. E. Oropeza, G. Gorni, M. Barawi, M. García-Tecedor, V. A. de la Peña O'Shea, J. P. Hofmann, J. Li, J. Kim, S. Cho, R. Wu and K. H. L. Zhang, *Nature Communications*, 2024, **15**, 5336.
12. F. Song, L. Bai, A. Moysiadou, S. Lee, C. Hu, L. Liardet and X. Hu, *Journal of the American Chemical Society*, 2018, **140**, 7748-7759.
13. Y. Zhang, Q. Fu, B. Song and P. Xu, *Accounts of Materials Research*, 2022, **3**, 1088-1100.
14. A. H. Shah, Z. Zhang, Z. Huang, S. Wang, G. Zhong, C. Wan, A. N. Alexandrova, Y. Huang and X. Duan, *Nature Catalysis*, 2022, **5**, 923-933.
15. H. Tan, B. Tang, Y. Lu, Q. Ji, L. Lv, H. Duan, N. Li, Y. Wang, S. Feng, Z. Li, C. Wang, F. Hu, Z. Sun and W. Yan, *Nature Communications*, 2022, **13**, 2024.
16. A. Mondal and A. Vomiero, *Advanced Functional Materials*, 2022, **32**, 2208994.
17. Q. Lu, Y. Yu, Q. Ma, B. Chen and H. Zhang, *Advanced Materials*, 2016, **28**, 1917-1933.
18. Y. Shi, Y. Zhou, D.-R. Yang, W.-X. Xu, C. Wang, F.-B. Wang, J.-J. Xu, X.-H. Xia and H.-Y. Chen, *Journal of the American Chemical Society*, 2017, **139**, 15479-15485.
19. Q. Li, O. K. Kucukosman, Q. Ma, J. Ouyang, P. Kucheryavy, H. Gu, C. L. Long, Z. Zhang, J. Young, J. V. Lockard, E. Garfunkel, J. Gao, W. Zhang and H. He, *ACS Catalysis*, 2024, **14**, 8899-8912.
20. X. Cao, J. E. Medvedeva and M. Nath, *ACS Applied Energy Materials*, 2020, **3**, 3092-3103.
21. S. Anantharaj, S. Kundu and S. Noda, *Journal of Materials Chemistry A*, 2020, **8**, 4174-4192.
22. W. Feng, W. Pang, Y. Xu, A. Guo, X. Gao, X. Qiu and W. Chen, *ChemElectroChem*, 2020, **7**, 31-54.
23. M. Das, G. Kumar and R. S. Dey, *ACS Applied Energy Materials*, 2022, **5**, 3915-3925.
24. Y. Wang, C. Han, L. Ma, T. Duan, Y. Du, J. Wu, J.-J. Zou, J. Gao, X.-D. Zhu and Y.-C. Zhang, *Small*, 2024, **20**, 2309448.
25. J. Zhang, C. Cheng, L. Xiao, C. Han, X. Zhao, P. Yin, C. Dong, H. Liu, X. Du and J. Yang, *Advanced Materials*, 2024, **36**, 2401880.
26. Y. Zhao, M. Cui, B. Zhang, S. Wei, X. Shi, K. Shan, J. Ma, G. Zhou and H. Pang, *Small Methods*, 2024, **8**, 2301465.
27. Y. Liu, Z. Tian, Q. Xu, Y. Yang, Y. Zheng, H. Pan, J. Chen, Z. Wang and W. Zheng, *ACS Applied Materials & Interfaces*, 2022, **14**, 8963-8973.
28. S. Esmailzadeh, T. Shahrabi, Y. Yaghoubinezhad and G. Barati Darband, *Journal of Colloid and Interface Science*, 2021, **600**, 324-337.
29. P. J. J. Sagayaraj, K. S, O. Keishi, N. Okibe, H.-i. Kim and K. Sekar, *Energy Advances*, 2025, DOI: 10.1039/D4YA00578C.
30. W. Du, Y. Shi, W. Zhou, Y. Yu and B. Zhang, *Angewandte Chemie International Edition*, 2021, **60**, 7051-7055.
31. S. Anantharaj, E. Subhashini, K. C. Swaathini, T. S. Amarnath, S. Chatterjee, K. Karthick and S. Kundu, *Applied Surface Science*, 2019, **487**, 1152-1158.
32. F. Wang, Y. Li, T. A. Shifa, K. Liu, F. Wang, Z. Wang, P. Xu, Q. Wang and J. He, *Angewandte Chemie International Edition*, 2016, **55**, 6919-6924.
33. J. Xu, J. Ruan, Y. Jian, J. Lao, Z. Li, F. Xie, Y. Jin, X. Yu, M.-H. Lee, Z. Wang, N. Wang and H. Meng, *Small*, 2024, **20**, 2305905.
34. I. Pathak, S. Prabhakaran, D. Acharya, K. Chhetri, A. Muthurasu, Y. R. Rosyara, T. Kim, T. H. Ko, D. H. Kim and H. Y. Kim, *Small*, 2024, **20**, 2406732.
35. A. Kareem, H. Mohanty, K. Thenmozhi, S. Pitchaimuthu and S. Senthilkumar, *ACS Applied Nano Materials*, 2024, **7**, 4886-4894.
36. A. Mikuła, M. Kożusznik, K. Mars, J. Cieślak, S. Sanden and U.-P. Apfel, *Chemistry of Materials*, 2024, **36**, 4571-4582.
37. M. Das, A. Biswas, Z. B. Khan and R. S. Dey, *Inorganic Chemistry*, 2022, **61**, 13218-13225.
38. M. B. Poudel, N. Logeshwaran, S. Prabhakaran, A. R. Kim, D. H. Kim and D. J. Yoo, *Advanced Materials*, 2024, **36**, 2305813.
39. B. Zhang, X. Li and M. Liu, *International Journal of Electrochemical Science*, 2024, 100579.
40. Š. Kment, A. Bakandritsos, I. Tantis, H. Kmentová, Y. Zuo, O. Henrotte, A. Naldoni, M. Otyepka, R. S. Varma and R. Zbořil, *Chemical Reviews*, 2024, **124**, 11767-11847.
41. W.-L. Mu, Y.-T. Luo, P.-K. Xia, Y.-L. Jia, P. Wang, Y. Pei and C. Liu, *Inorganic Chemistry*, 2024, **63**, 6767-6775.
42. Y. Du, Q. Li, L. Han, P. Yang, L. Xin, W. Jin, W. Xiao, Z. Li, J. Wang, Z. Wu and L. Wang, *Applied Catalysis B: Environment and Energy*, 2024, **344**, 123617.
43. J. Tymoczko, F. Calle-Vallejo, W. Schuhmann and A. S. Bandarenka, *Nature Communications*, 2016, **7**, 10990.
44. J. Yu, S. Zhang, Y. Liu, Y. Tong, Y. Zhong, B. He, E. Hu, J. Zhang and Z. Chen, *ACS Materials Letters*, 2024, **6**, 4719-4727.
45. M. Guo, S. Chen, Y. Xiong, M. Chen, J. Xia, W. Chen, H. Zheng, X. Jiang and X. Qian, *Journal of Alloys and Compounds*, 2024, **1001**, 175094.
46. Y. Ma, L. Yang, Y. Li, H. Li, Y. Huang and J. Chen, *Small*, 2024, **20**, 2308650.
47. J. Dai, D. Zhao, W. Sun, X. Zhu, L.-J. Ma, Z. Wu, C. Yang, Z. Cui, L. Li and S. Chen, *ACS Catalysis*, 2019, **9**, 10761-10772.
48. W. Hu, L. Xie, C. Gu, W. Zheng, Y. Tu, H. Yu, B. Huang and L. Wang, *Coordination Chemistry Reviews*, 2024, **506**, 215715.

View Article Online
DOI: 10.1039/D5TA04391C

49. C. Yang, J. Yue, G. Wang and W. Luo, *Angewandte Chemie*, 2024, **136**, e202401453.
50. K. Fan, L. Zong, J. Liu, C.-H. Chuang, M. Dong, Y. Zou, Y. Xu, H. Q. Fu, L. Zhang, L. Wang, M. Zhou, T. Zhan, P. Liu and H. Zhao, *Advanced Energy Materials*, 2024, **14**, 2400052.
51. L. Zhou, C. Yang, W. Zhu, R. Li, X. Pang, Y. Zhen, C. Wang, L. Gao, F. Fu, Z. Gao and Y. Liang, *Advanced Energy Materials*, 2022, **12**, 2202367.
52. S. Anantharaj and S. Noda, *International Journal of Hydrogen Energy*, 2020, **45**, 15763-15784.
53. R. E. Mostafa, S. S. Mahmoud, N. S. Tantawy and S. G. Mohamed, *ChemNanoMat*, 2024, **10**, e202300610.
54. P. Wang, X. Zhang, J. Zhang, S. Wan, S. Guo, G. Lu, J. Yao and X. Huang, *Nature communications*, 2017, **8**, 14580.
55. D. Cao, J. Shao, Y. Cui, L. Zhang and D. Cheng, *Small*, 2023, **19**, 2301613.
56. S. Anantharaj, S. Noda, M. Driess and P. W. Menezes, *ACS Energy Letters*, 2021, **6**, 1607-1611.
57. H. Zhang, B. Yang, X. Wu, Z. Li, L. Lei and X. Zhang, *ACS Applied Materials & Interfaces*, 2015, **7**, 1772-1779.
58. T. Shinagawa, A. T. Garcia-Esparza and K. Takanabe, *Scientific reports*, 2015, **5**, 13801.
59. D. Yu, Z. Li, G. Zhao, H. Zhang, H. Aslan, J. Li, F. Sun, L. Zhu, B. Du, B. Yang, W. Cao, Y. Sun, F. Besenbacher and M. Yu, *ChemSusChem*, 2020, **13**, 260-266.
60. B. Xu, Z. Chen, X. Yang, X. Wang, Y. Huang and C. Li, *Chemical Communications*, 2018, **54**, 9075-9078.
61. L. Zhai, T. W. Benedict Lo, Z.-L. Xu, J. Potter, J. Mo, X. Guo, C. C. Tang, S. C. Edman Tsang and S. P. Lau, *ACS Energy Letters*, 2020, **5**, 2483-2491.
62. X. Jian, W. Zhang, Y. Yang, Z. Li, H. Pan, Q. Gao and H.-J. Lin, *ACS Catalysis*, 2024, **14**, 2816-2827.

View Article Online
DOI: 10.1039/D5TA04391C

The data supporting this article have been included as part of the manuscript and Supplementary Information.